Journal of Molecular Catalysis A: Chemical 385 (2014) 149–159

Contents lists available at ScienceDirect

Journal of Molecular Catalysis A: Chemical

journal homepage: www.elsevier.com/locate/molcata

A solution-phase synthesis of supported Ni_2P catalysts with high activity for hydrodesulfurization of dibenzothiophene

Hua Song[a,b], Min Dai[c], Hua-Lin Song[d,*], Xia Wan[c], Xiao-Wei Xu[a], Zai-Shun Jin[d]

[a] College of Chemistry and Chemical Engineering, Northeast Petroleum University, Daqing 163318, China
[b] Provincial Key Laboratory of Oil & Gas Chemical Technology, College of Chemistry & Chemical Engineering, Northeast Petroleum University, Daqing 163318, Heilongjing, China
[c] Xinjiang Petroleum Investigation Design and Research Institute (Co., Ltd.), Karamay 834000, Xinjiang, China
[d] Key Laboratory of Cancer Prevention and Treatment of Heilongjiang Province, Mudanjiang Medical University, Mudanjiang 157011, Heilongjing, China

ARTICLE INFO

Article history:
Received 9 October 2013
Received in revised form 23 January 2014
Accepted 25 January 2014
Available online 3 February 2014

Keywords:
Nickel phosphide
Hydrodesulfurization
Dibenzothiophene
Triphenylphosphine
Nickel acetylacetonate

ABSTRACT

A novel solution-phase low temperature synthesis of a supported Ni_2P catalyst is described. This uses nickel acetylacetonate ($Ni(acac)_2$) and low cost triphenylphosphine (TPP) in the presence of the coordinating solvent tri-*n*-octylamine (TOA) to form Ni_2P/MCM-41 catalysts. The catalysts were characterized by X-ray diffraction (XRD), N_2-adsorption specific surface area measurements (BET), CO uptake, transmission electron microscopy (TEM), Fourier transform infrared spectroscopy (FT-IR) and X-ray photoelectron spectroscopy (XPS). The effects of the synthesis temperature, and initial P/Ni molar ratio on the formation of the Ni_2P phase were studied. The formation of the crystalline phase follows the order $Ni < Ni_{12}P_5 < Ni_2P$ with increasing synthesis temperature. The high initial P/Ni molar ratio favored the formation and dispersion of the Ni_2P phase, and a mixture of the $Ni_{12}P_5$ and Ni_2P phases was observed in the sample with the low initial P/Ni molar ratio of 0.5. The dibenzothiophene (DBT) hydrodesulfurization (HDS) activity increased with reaction temperature in all cases. The catalysts synthesized at 603 K with an initial P/Ni molar ratio of 6 exhibited good DBT HDS activity. The DBT conversion was close to 100% at 613 K, which was much higher than that of the catalyst prepared by the conventional temperature programmed reduction (TPR) method (DBT conversion 43%). During the HDS reaction, the superficial phosphosulfide phase $Ni_xP_yS_z$ was formed on the surface of the catalyst; this showed higher activity than Ni_2P.

1. Introduction

Driven by the growing demand for fuel oil and the increasing use of heavy crude oil, sulfur removal from fuels has attracted a great deal of attention, and will continue to do so in the coming years. Moreover, more and more rigorous environmental regulations limiting the emissions of sulfur dioxide and the continuing decline in the quality of petroleum feedstocks have made sulfur removal a serious problem in the refining industry. It has been recognized that current commercial hydrodesulfurization (HDS) catalysts are not adequate to meet the regulated levels, and the challenge of producing ultra clean fuels has stimulated the investigation and development of high-performance HDS catalysts. Much of the research over the past decade has been aimed at improving the classic catalysts, which are based on molybdenum sulfide promoted by cobalt or nickel [1–3], as well as at finding novel catalyst materials. Transition metal phosphides (i.e. MoP, WP, Fe_2P, Ni_2P) have been found quite promising as alternative hydrodesulfurization catalysts because of their high HDS activity and stability [4–6]. Ni_2P is a transition metal phosphide (TMP) that has physical properties, such as hardness and strength, close to ceramics, yet has the electrical properties of metals, such as its conductivity and Hall coefficient [5,7–9]. The catalyst Ni_2P shows the most remarkable activities of all the phosphides and has attracted considerable attention for its widespread applications in HDS research [5–7,10,11].

All recent reports of Ni_2P catalysts have described catalyst production by temperature programmed reduction (TPR) of a mixture of the metal nickel salt with ammonium phosphate in hydrogen [4,12,13]. The nickel phosphate precursor is prepared mainly by impregnation of the support with $(NH_4)_2HPO_4$ (or $NH_4H_2PO_4$) and $Ni(NO_3)_2$ solutions, followed by drying and calcination. After a subsequent temperature programmed reduction in hydrogen, the desired Ni_2P catalyst is formed. The method of temperature programmed reduction is convenient and simple, but has the disadvantage of requiring a high reduction temperature. Berhault et al. [14] had observed that the reduction of phosphate

* Corresponding author at: Key Laboratory of Cancer Prevention and Treatment of Heilongjiang Province, Mudanjiang Medical University, Mudanjiang 157011, Heilongjing, China. Fax: +86 0453 6984321.
E-mail addresses: songhua2004@sina.com (H. Song), songhualin401@126.com (H.-L. Song).

1381-1169/$ – see front matter © 2014 Published by Elsevier B.V.
http://dx.doi.org/10.1016/j.molcata.2014.01.019

to phosphide did not start until the temperature reached 823 K and led to the selective formation of the Ni_2P phase at 923 K. The P—O bond is strong, and its reduction requires high temperature. Moreover, hydrogen atoms are available only after the metallic nickel particles have been formed and dissociate hydrogen molecules to hydrogen atoms [15]. These active hydrogen atoms can spill over to the phosphate and reduce it to phosphorus or phosphine. The phosphorus or phosphine can then react with the metal particles to form Ni_2P. The strong P—O bond and the surface diffusion of the H atoms are responsible for the high reduction temperature, which leads to large catalyst particles, relatively low catalytic activity and the almost exclusive formation of phosphorus [15]. It is therefore necessary to explore novel approaches featuring mild conditions for preparing the Ni_2P catalyst. Recently, there have been reports of some new approaches to preparing Ni_2P such as solvothermal reactions [16,17], thermal decomposition of nickel thiophosphate ($NiPS_3$) [18], reduction of nickel dihydrogenphosphite [19], thermal decomposition of a mixture of trioctylphosphine (TOP) with metal salts or metal hypophosphites precursors in solution-phase, plasma methods [20], and co-reaction of metal or metal oxide with phosphines [21,22]. Of all these methods, the solution-phase process, which uses trioctylphosphine (TOP) and tris(trimethylsilyl)phosphine as phosphorus reagents, is particularly noteworthy [23–29]. However, the high price of these two phosphorus reagents limits the use of these methods to prepare Ni_2P catalysts, and most current reports about the solution-phase synthesis of Ni_2P have been limited to theoretical research into nanophase materials. Hence, it is essential to find a low cost phosphorus reagent to replace the TOP and tris(trimethylsilyl)phosphine and to synthesize Ni_2P for HDS research using a solution-phase process.

In this paper, we demonstrate a low cost solution-phase method for preparing supported Ni_2P catalyst using mild conditions. The method uses nickel acetylacetonate ($Ni(acac)_2$) as a nickel precursor, the low-price triphenylphosphine (TPP) as a phosphorus precursor, and tri-*n*-octylamine (TOA) as a coordinating solvent. The catalysts were synthesized at 603 K in a N_2 atmosphere. By comparison, preparation of the catalyst using the conventional TPR method requires a reduction temperature exceeding 873 K so these conditions are extremely mild, yet the DBT conversion is high. The phosphorus precursor and TOA used in our approach are cheaper than tri-*n*-octylphosphine (TOP) and oleylamine (OA) which have been widely used in the current solution-phase approach for the synthesis of nanocrystalline Ni_2P. The effects of the P/Ni molar ratio and synthesis temperature on the formation of Ni_2P phase were studied. The results show that a highly dispersed and active Ni_2P catalyst can be obtained.

2. Experimental

2.1. Synthesis of catalysts

Siliceous MCM-41 support was synthesized using tetraethyl orthosilicate (TEOS) as the silica source and cetyltrimethylammonium bromide (CTAB) as the template, following the procedure as described in the literature [30].

The synthesis process of supported Ni_2P catalysts were carried out in an organic solution at a mild temperature under N_2 atmosphere (99.99%). The catalysts, with different initial P/Ni molar ratios of 0.5, 2, 6, and 10, were prepared with Ni metal loading of 12 wt.%. In a typical synthesis technique, a mixture of TOA (40 mL, 98%), $Ni(acac)_2$ (0.26 g, 99%), TPP (0.55 g, 99%), and MCM-41 (0.85 g, 99.9%) were stirred magnetically at 393 K for 30 min (the initial molar ratio of P/Ni is 2), and then heated up to 603 K at a rate of 10 K min^{-1}, held for 2 h, then naturally cooled to room temperature (The heating and cooling processes were carried out in a continuous N_2 flow). The obtained dark suspension was passivated in O_2/N_2 mixture (0.5 vol.% of O_2) with flowrate of 20 mL/min for 2 h under vigorous stirring, and then treated with 50 mL of ethanol to form black precipitate, which was isolated by filtering, washed fully with ethanol and carbon tetrachloride. The whole experiment process was operated in atmospheric pressure. The catalysts obtained were named Ni-P(X)/MCM, where X is the initial P/Ni molar ratio.

The structural property and catalytic activity of the Ni_2P catalysts prepared by solution-phase synthesis was compared with the catalyst prepared by conventional TPR method. For the TPR method, the catalyst precursors were prepared by a standard incipient wetness impregnation of an ammonium dihydrogen phosphate ($NH_4H_2PO_4$) and nickel nitrate hexahydrate ($Ni(NO_3)_2{\cdot}6H_2O$) solution with MCM-41. The impregnated solids were dried at 393 K for 10 h and calcined at 773 K for 3 h, and then directly reduced in a fixed-bed reactor by heating to 973 K at a rate of 2 K min^{-1} in a flow of H_2 (200 mL/min), held for 2 h, then naturally cooled to room temperature in a continuous H_2 flow. The obtained catalyst was passivated in O_2/N_2 mixture (0.5 vol.% of O_2) with flowrate of 20 mL/min for 2 h. Oyama et al. [31] have synthesized a series of SiO_2-supported nickel phosphide catalysts with different initial Ni/P ratios by TPR, and found the catalyst with initial Ni/P ratio of about 1/2 (actual Ni/P = 1/0.57 after reaction) corresponded to a pure Ni_2P phase with an excellent activity. Hence, in our experiment, the Ni metal loading of the catalyst prepared by TPR was determined as 12 wt.% and initial P/Ni molar ratio was determined as 2. The catalysts obtained were named Ni-P(2)/MCM-T.

2.2. Characterization of catalysts

X-ray diffraction (XRD) analysis of the samples were carried out on a D/max-2200PC-X-ray diffractometer using CuKα radiation under the setting conditions of 40 kV, 30 mA, scan range from 10 to 80° at a rate of 10°/min.

The typical physico-chemical properties of supports and catalysts were analyzed by BET method using Micromeritics adsorption equipment of NOVA2000e. All the samples were outgassed at 473 K until the vacuum pressure was 6 mm Hg. The adsorption isotherms for nitrogen were measured at 77 K.

The CO uptake was measured using pulsed chemisorption. About 1.0 g of catalyst was pretreated in a quartz reactor to remove the passivation layer by heating up to 773 K at a rate of 2 K min^{-1} in H_2 with flowrate of 20 mL/min for 2 h, and then naturally cooled to room temperature in a continuous H_2 flow and an He flow at 30 mL/min was used to flush the catalyst for 30 min to achieve an adsorbate-free. After pretreatment, 1-mL pulses of CO were injected into a flow of He (30 mL/min), and the CO uptake was measured using a TCD. CO pulses were repeatedly injected until the response from the detector showed no further CO uptake after consecutive injections. Assuming a 1:1 adsorption stoichiometry between CO and metal atoms, this value corresponds to the metal site density on the catalyst surface.

Transmission electron microscopy (TEM) studies were performed using the JEM-1010 instrument supplied by JEOL. The samples were dispersed in ethanol and placed on a carbon grid before TEM examinations.

Infrared absorption spectroscopy (IR) was acquired in the range of 400–4000 cm^{-1}. The solid specimens were generated via the conventional procedure, i.e. by the pelletizing 1.5 mg of the catalyst with 500 mg of KBr.

The X-ray photoelectron spectroscopy (XPS) spectra were acquired using ESCALAB MKII spectrometer. XPS measurements have been performed using monochromatic Mg K_α radiation (E = 1253.6 eV) and equipped with a hemi-spherical analyzer operating at fixed pass energy of 40 eV. The recorded photoelectron

binding energies were referenced against the C 1s contamination line at 284.8 eV, and the depth of the data collected was 1–3 nm.

2.3. Catalytic activities

The HDS of DBT was carried out in a high-pressure fixed-bed reactor (9 mm in diameter, and 300 mm in length) using a feed consisting of a decalin solution of DBT (1 wt.%). Catalytic activities were measured at different temperatures (553–613 K), 3.0 MPa of H_2, hydrogen/oil ratio of 500 (v/v) and weight hourly space velocities (WHSV) of 4 h^{-1}. The catalyst was pressed in discs, crushed and sieved with 30–60 mesh. Prior to reaction, 0.5 g of the catalysts were pretreated in situ with flowing H_2 (40 mL/min) at 613 K for 2 h. The evolution of the reaction was studied by collecting liquid samples after 2 h at the desired reaction temperature. The liquid samples were collected every hour and analyzed by FID gas chromatography with a GC-14C-60 column.

Turnover frequency (TOF) values of the samples containing nickel phosphide were calculated using Eq. (1) [32]:

$$\mathrm{TOF} = \frac{F}{W}\frac{X}{M} \quad (1)$$

where F is the molar rate of DBT fed into the reactor (μmol s^{-1}), W is the weight of catalyst (g), X is the conversion of DBT (%), and M is the mole of sites loaded.

3. Results and discussion

3.1. Characterization of catalysts

3.1.1. XRD

In order to study the effect of reaction temperature on the formation of the catalyst crystalline phases, the XRD patterns of MCM-41 supported samples with an initial P/Ni molar ratio of 6, obtained at different synthesis temperatures, were carried out, with the results shown in Fig. 1. It can be seen that from 393 K to 483 K, no crystalline phase is observed except the MCM-41 support, with a broad peak at $2\theta = 25^\circ$. This means that the Ni and P species exist in noncrystalline

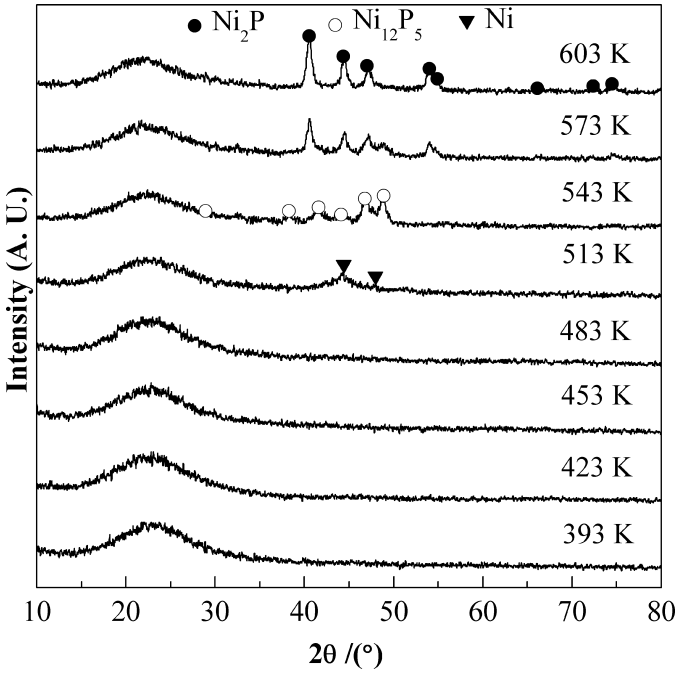

Fig. 1. XRD patterns of MCM-41 supported samples with initial P/Ni molar ratio of 6 and obtained at different synthesis temperature.

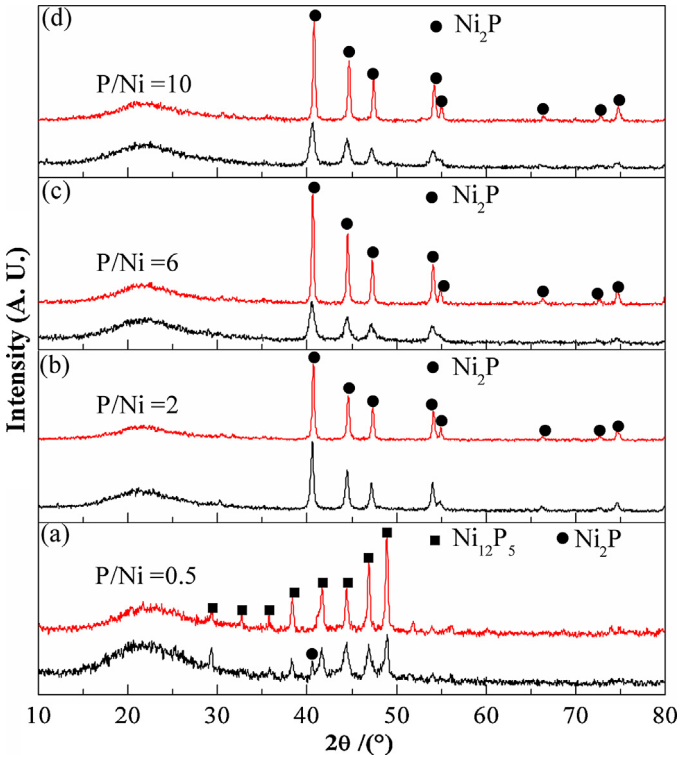

Fig. 2. XRD patterns of the fresh and spent MCM-41 supported samples with different initial P/Ni molar ratio. The lower and upper lines are fresh and spent samples, respectively.

forms over this synthesis temperature range. At a synthesis temperature of 513 K, two diffraction peaks, at $2\theta = 44.4^\circ$ and 51.8°, can be observed, corresponding to the Ni metal phase (PDF 65-2865). When the synthesis temperature was increased to 543 K, the Ni phase disappeared, and the $Ni_{12}P_5$ phase was observed, with peaks at $2\theta = 32.6^\circ$, 38.4°, 41.7°, 44.4°, 46.9° and 48.9° (PDF 22-1190). Subsequently, the Ni_2P phase is observed as the synthesis temperature is increased to 573 K. This produces weak peaks at $2\theta = 40.6^\circ$, 44.5°, 47.1°, 54.1°, 54.8°, 66.1°, 72.5° and 74.5° (PDF 03-0953). At 603 K, some strong diffraction peaks of the Ni_2P phase are detected, which indicates that more Ni_2P phase is formed and the crystallinity of the Ni_2P is improved with increasing synthesis temperature. The XRD analysis results show that, with the increase of synthesis temperature, the crystalline phases appeared follows the order Ni, $Ni_{12}P_5$, and Ni_2P. Ni and $Ni_{12}P_5$ are the reactive intermediates leading to Ni_2P, and, in comparison with Ni_2P phase, Ni and $Ni_{12}P_5$ might form under milder conditions, whereas the conversion to Ni_2P requires higher temperatures.

The initial P/Ni molar ratio is known to control the Ni_2P particle size and is the key factor in determining its structure [31,32]. TPP can work as a reducing agent for the Ni precursor, as well as a source of phosphorus through cleavage of P—C bonds [33]. In order to study the effect of initial P/Ni molar ratio on the solution-phase synthesis, XRD patterns of catalysts with initial P/Ni molar ratios in the range 0.5–10 have been investigated, and the results are shown in Fig. 2 (dark lines in each frame). $Ni_{12}P_5$ and Ni_2P phases are observed in the sample with an initial P/Ni molar ratio of 0.5 (Fig. 2(a)), while the samples with higher initial P/Ni molar ratios exhibit only the Ni_2P phase. The formation of $Ni_{12}P_5$ with a low proportion of P is understandable, as $Ni_{12}P_5$ contains a lower proportion of P than does Ni_2P. The Ni_2P peaks become weaker with the increase of initial P/Ni molar ratio. The peak width indicates the formation of smaller crystallites of Ni_2P with the increase in P content (see Table 1), and it is a likely consequence of a better dispersion of the Ni_2P particles,

Table 1
Properties of catalyst samples.

Sample	S_{BET} ($m^2\ g^{-1}$)	V_p ($cm^3\ g^{-1}$)	d_p (av) (nm)	XRD phase	D_c (nm)[c]	CO uptake ($\mu mol\ g^{-1}$)	Metal site density[d] ($\mu mol\ g^{-1}$)
MCM-41	1012	0.816	3.2	–		–	–
Ni-P(0.5)/MCM[a]	712	0.503	2.8	$Ni_2P + Ni_{12}P_5$	3($Ni_{12}P_5$)	156	2227($Ni_{12}P_5$)
Ni-P(0.5)/MCM[b]	–	–	–	$Ni_{12}P_5$	8	101	278
Ni-P(2)/MCM[a]	690	0.472	2.7	Ni_2P	10	97	223
Ni-P(2)/MCM[b]	–	–	–	Ni_2P	12	78	186
Ni-P(6)/MCM[a]	668	0.456	2.7	Ni_2P	5	124	742
Ni-P(6)/MCM[b]	–	–	–	Ni_2P	10	83	223
Ni-P(10)/MCM[a]	613	0.417	2.7	Ni_2P	4	132	1114
Ni-P(10)/MCM[b]	–	–	–	Ni_2P	11	86	202
Ni-P(2)/MCM-T[a]	398	0.239	2.4	Ni_2P	18	43	124
Ni-P(2)/MCM-T[b]	–	–	–	Ni_2P	20	39	111

[a] Fresh sample.
[b] Spent sample.
[c] Calculated from the $D_c = K\lambda/\beta\cos(\theta)$ (Scherrer equation) base on the Ni_2P or $Ni_{12}P_5$ {1 1 1}.
[d] Calculated from the $L = S\tilde{n}f$, where f is the fractional weight loading of the sample ($g_{nickel\ phosphide}/g_{cat.}$) and $\tilde{n}$ is the average surface metal atom density, which for Ni_2P is 1.01×10^{15} atoms cm^{-2}, S is the effective surface area of the crystallites (assuming cubic or spherical geometry) and which can be calculated from the $S = 6/\rho D_c$ (ρ is the density of nickel phosphides taken as 7.09 g cm^{-1}) [31].

which are easier to form with higher P contents. The reason for this phenomenon can be understood since the Ni component is able to disperse itself better during the reaction stage when there are larger amounts of TPP on the surface. These results demonstrate that the P/Ni molar ratio has a significant influence on the nature of the phase formed. Ni_2P cannot be formed with the low P/Ni molar ratio of 0.5, possibly because a proportion of the P species could not participate in the reduction of the Ni precursor or because some P—C bonds did not break. The crystallite size calculated from Scherrer's equation is a mean value and is also listed in Table 1.

XRD patterns were also obtained for the spent samples (Fig. 2, red lines in each frame). For all the samples, the $Ni_{12}P_5$ and Ni_2P phase became more crystalline after the hydrotreatment reaction. This is understandable since there is prolonged exposure at the hydrotreatment temperature of 613 K, indicating that the smaller $Ni_{12}P_5$ and Ni_2P particles are not stable at this temperature. For the sample with an initial Ni/P ratio of 0.5, the XRD pattern after reaction shows that the Ni_2P phase has completely disappeared. It is likely that this sample is phosphorus deficient, and the prolonged exposure at 613 K has caused the Ni_2P phase to turn into the $Ni_{12}P_5$ phase. It is also possible that the sample loses some phosphorus during the hydrotreatment reaction. In addition, no other new phase can be observed in the spent samples, implying that the main catalytic framework of $Ni_{12}P_5$ and Ni_2P remains unchanged.

3.1.2. FT-IR

In order to study the formation of Ni_2P catalysts, FT-IR characterizations of catalysts with an initial P/Ni molar ratio of 6 synthesized at different temperature were performed (Fig. 3). The FT-IR spectrum of every sample shows a broad strong signal above 1080 cm^{-1}, which can be assigned to the Ni bound P═O stretching band, a natural consequence of surface oxidation resulting from handling of samples in the open air. This observation is similar to the results reported by Carenco et al. [25] and Senevirathne et al. [34]. Three peaks at 1450–1600 cm^{-1} are observed in the catalysts obtained when the synthesis temperature is below 513 K. These peaks are attributed to the symmetric stretching vibrations of C═C in the fundamental ring of the aromatics derived from coordinated TPP. However, these peaks do not appear in the catalysts obtained at synthesis temperatures higher than 513 K. This indicates that the P—C bond of TPP is broken at about 513 K, and the aromatic products formed are washed out by ethanol and carbon tetrachloride. Moreover, peaks from the C—H stretching vibrations can be observed at 2925 and 2852 cm^{-1}, which result from an aliphatic chain remaining on the surface of the particles after washing. This organic residue probably results from the reaction of TOA with the $Ni(acac)_2$ fragment and is relatively weakly bound to the surface, since its vibration modes are not affected by the proximity of metal [34].

3.1.3. Textural properties

Table 1 summarizes the textural properties of Ni-P(X)/MCM and Ni-P(2)/MCM-T catalysts, as well as that of the MCM-41 support. The surface area and pore volume of the MCM-41 support are 1012 $m^2\ g^{-1}$ and 0.816 $cm^3\ g^{-1}$, respectively. It can be seen that all of the catalysts suffer a decrease in the specific surface areas and pore volumes after metal phosphide formation. It is also noteworthy that the average pore diameter of the catalysts is smaller than that of the MCM-41 support. The decrease of the average pore diameter may be due to the deposition of Ni species on the surface of MCM-41 support. The BET surface areas of all the Ni-P(X)/MCM catalysts ranged from 613 to 712 $m^2\ g^{-1}$, a relatively small variation with initial P/Ni molar ratio, and are higher than that of the catalyst prepared by the TPR method. This implies that the initial P/Ni

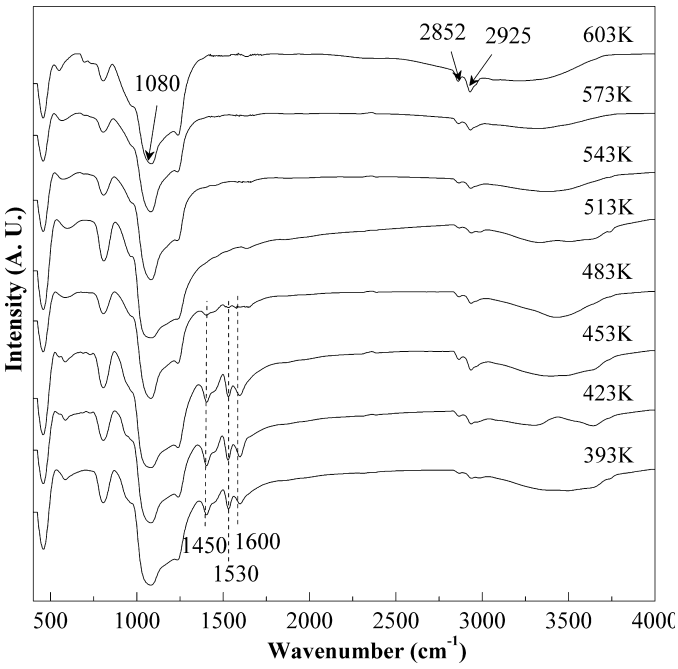

Fig. 3. FTIR spectra for the catalysts with initial P/Ni molar of 6 and synthetized at 393–603 K.

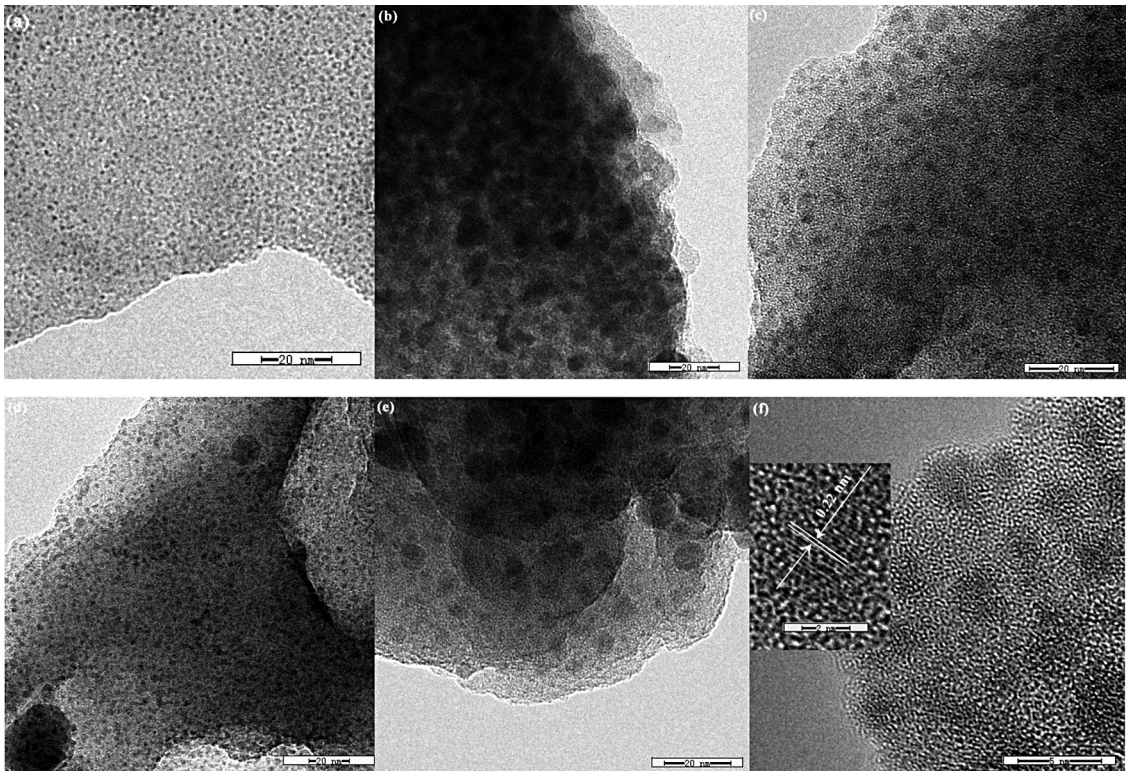

Fig. 4. Low and high resolution TEM micrographs of the catalysts. (a) Ni-P(0.5)/MCM, (b) Ni-P(2)/MCM, (c) Ni-P(6)/MCM, (d) Ni-P(10)/MCM, (e) Ni-P(2)/MCM-T, (f) high resolution TEM micrographs of Ni-P(6)/MCM.

molar ratio has little effect on the textural properties prepared by solution-phase synthesis and any that is observed may be due to the excess P species that can be washed away by ethanol and carbon tetrachloride. However, our previous study found that the textural properties of catalysts prepared by TPR were closely associated with the P content in the precursor, because the excess P evolved during the reduction covers the outer surface of the catalysts, leading to a significant decrease in the surface areas and pore volumes [35]. Oyama et al. [31] also reported that high P loadings resulted in low surface areas of the supported Ni_2P catalysts obtained by the TPR method. Furthermore, Abu et al. [36] found that the partial structure of MCM-41 is destroyed during the preparation of metal phosphide by the TPR method, resulting in the metal phosphide supported MCM-41 having much lower surface areas than pristine MCM-41. Clearly, high surface areas and pore volumes of MCM-41-supported Ni_2P catalysts are more readily available using our proposed solution-phase synthesis.

3.1.4. CO uptake

Metal phosphide can be titrated by CO chemisorption at room temperature [5]. CO uptake measurements were used to titrate the surface metal atoms and to provide an estimate of the metal sites and dispersion on the catalysts (assuming a stoichiometry of one CO molecule per surface Ni atom) [31]. The measured CO adsorption capacities are presented in Table 1. It is clear that fresh samples prepared by the proposed solution-phase synthesis show high values of CO uptake, at least two times higher than that of the catalyst prepared by TPR method. This is attributed to the smaller particles of Ni-P(X)/MCM (as shown in Table 1), and also indicates a better dispersion of Ni_2P particles in the Ni-P(X)/MCM catalysts. Significantly lower CO uptake of the Ni-P(2)/MCM-T catalyst is observed and is possibly caused by the poor dispersion of Ni_2P particles in this catalyst or by having its surface blocked by phosphates, which reduces the amounts of CO adsorption. This will be discussed later with the XPS results. CO molecules may also be adsorbed on P sites, but their numbers are very small and they can be ignored [37]. Of all the fresh Ni-P(X)/MCM catalysts, the Ni-P(0.5)/MCM catalyst shows the highest value of CO uptake, which implies that the mixture phases of $Ni_{12}P_5$ and Ni_2P have a better dispersion than that of the pure Ni_2P phase. This result is similar to that reported by Korányi et al. [38]. Moreover, it should be noted that the CO uptakes of spent Ni-P(X)/MCM catalysts show a dramatic reduction compared to the fresh samples. This indicates that the dispersion of the Ni-P(X)/MCM catalysts has dropped during the HDS reaction. The crystallite size obtained from XRD also shows that the particles in the Ni-P(X)/MCM catalysts become bigger. Although the CO uptakes of spent Ni-P(X)/MCM catalysts suffer a decrease, their values are still higher than that of Ni-P(2)/MCM-T. It can also be seen that the CO uptake values are below the theoretical surface metal site density calculated from the average particle size determined from the XRD line-broadening of the catalysts. This indicates that some metal sites may be blocked by excess phosphorus, since the surfaces of all the catalysts are rich in phosphorus. This will also be discussed with the XPS analysis

3.1.5. TEM

Distinct differences in the morphologies and particle sizes of the catalysts can be seen in the TEM images (Fig. 4). Clearly, unlike the typical stacked morphologies of the Mo and W sulfides, the nickel phosphide is not layered and forms spherical particles that can be well dispersed on supports [39]. It can be seen that the TEM images of catalysts prepared by the proposed solution-phase synthesis (Fig. 4(a)–(d)) exhibit similar particle size distribution, while the catalyst prepared by the TPR method exhibits a larger particle size distribution (Fig. 4(e)). This indicates the catalysts prepared by the solution-phase synthesis present a good dispersion of nanoparticles on the MCM-41 support. Of all the catalysts prepared by the solution-phase synthesis, the Ni-P(0.5)/MCM catalyst, containing predominantly $Ni_{12}P_5$ with a minor amount of Ni_2P, shows the smallest particle size, in the range 1–2 nm, and appears to be the

most homogeneous. This indicates that the $Ni_{12}P_5$ phase has better dispersion than that of the Ni_2P phase, a feature which is also confirmed by the CO uptake results in Table 1. Furthermore, the morphology of the Ni_2P particles is found to be highly dependent on the initial P content. Fig. 4(b) and (c) shows that the diameter of the Ni_2P particles decreases from 8–12 nm to 3–4 nm as the P/Ni molar ratio increases from 2 to 6 and may be because the higher P content helps to disperse the Ni species. With increasing initial P/Ni molar ratio, up to 10, the diameter of the Ni_2P particles did not change much (Fig. 4(d)). Fig. 4(f) shows a lattice spacing of about 0.22 nm, consistent with the *d*-spacing value for the {1 1 1} crystallographic planes of the Ni_2P phase. The particles derived from TEM and those calculated from XRD are in reasonable agreement (Table 1).

3.1.6. XPS

In order to gain further insight into the properties of the surfaces of fresh and spent catalysts, the XPS technique was employed. XPS spectra in the Ni(2p) and P(2p) regions for the fresh and spent catalysts are shown in Fig. 5, and the binding energies are presented

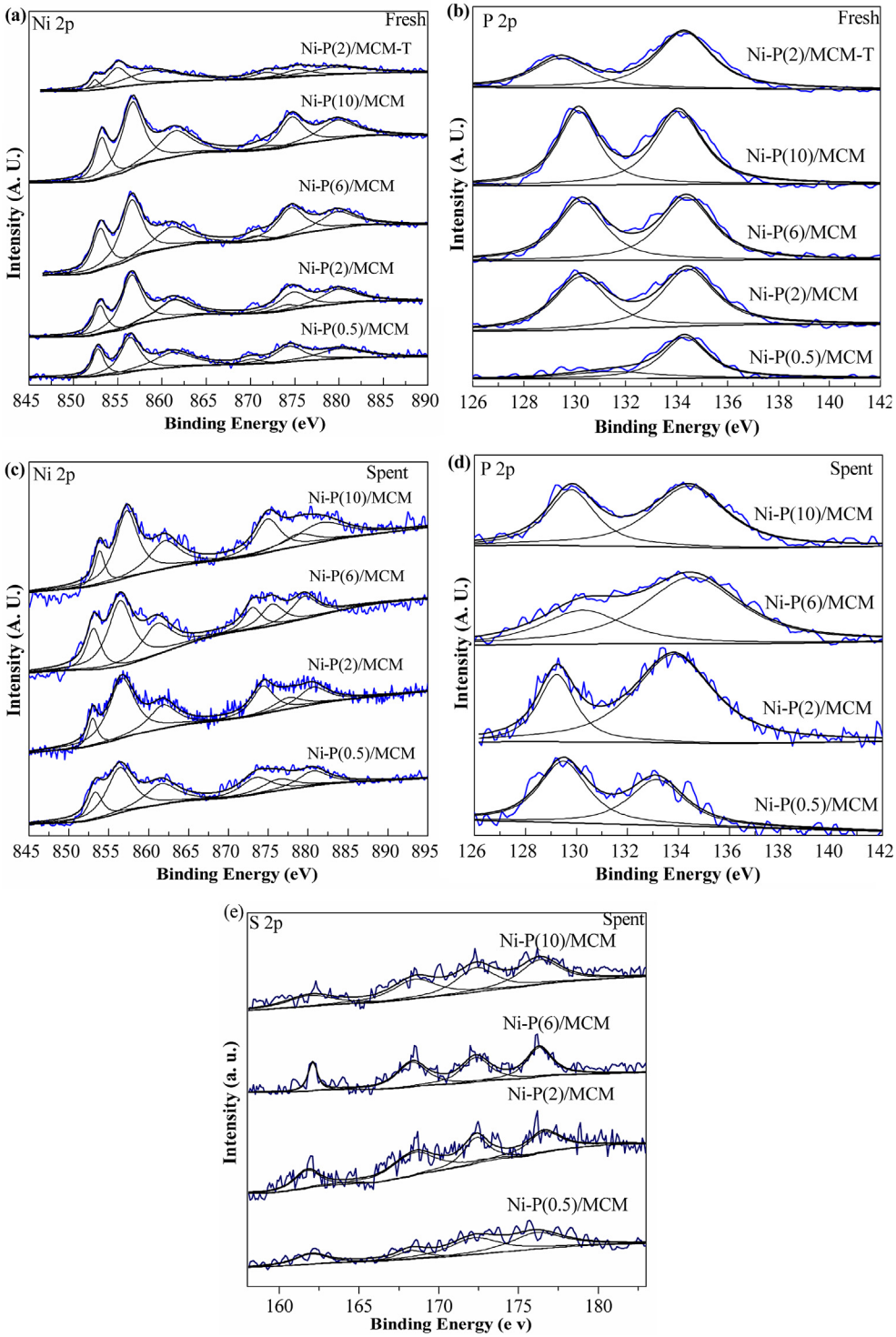

Fig. 5. XPS spectra in the Ni(2p), P(2p) and S(2p) regions for the fresh and spent catalysts.

Table 2
XPS binding energies and superficial concentrations (X = Ni + P + S) for the fresh and spent catalysts.

Sample	Binding energy (eV)						Superficial atomic ratio[c]					
	Ni $2p_{3/2}$			P 2p		S $2p_{3/2}$	$\frac{Ni^{\delta+}}{\sum Ni}$	P/Ni	Ni/X	P/X	S/X	Ni/Si
	Ni^{2+}	Satellite	$Ni^{\delta+}$	P^{5+}	$P^{\delta-}$	Sulfide						
Ni-P(0.5)/MCM[a]	856.4	861.7	852.7	134.3	129.3	–	0.321	1.6	0.379	0.621	–	0.135
Ni-P(0.5)/MCM[b]	856.4	861.6	853.2	134.1	129.2	161.9	0.222	0.8	0.316	0.263	0.421	0.099
Ni-P(2)/MCM[a]	856.6	861.8	852.9	134.5	130.1	–	0.349	2.4	0.277	0.658	–	0.174
Ni-P(2)/MCM[b]	856.6	861.8	853.0	134.0	129.2	161.4	0.307	2.2	0.193	0.425	0.382	0.137
Ni-P(6)/MCM[a]	856.7	862.0	853.0	134.4	130.1	–	0.402	2.3	0.303	0.697	–	0.194
Ni-P(6)/MCM[b]	856.8	862.1	853.1	134.3	130.0	161.6	0.371	2.2	0.187	0.408	0.345	0.104
Ni-P(10)/MCM[a]	856.9	862.3	853.2	134.1	129.9	–	0.393	2.6	0.278	0.722	–	0.276
Ni-P(10)/MCM[b]	857.2	862.0	853.4	134.4	129.8	161.6	0.386	2.3	0.177	0.412	0.348	0.090
Ni-P(2)/MCM-T[a]	856.1	860.2	852.8	134.8	129.6	–	0.230	3.9	0.208	0.812	–	0.578

[a] Fresh sample.
[b] Spent sample.
[c] The atomic ratios estimated from the ratios of total areas of corresponding element (all valencies) peaks which were detected by the XPS analytical instrument.

in Table 2. As shown in Fig. 5(a), all spectra were decomposed, taking into account the spin-orbital splitting of the Ni $2p_{3/2}$ and Ni $2p_{1/2}$ lines (about 17 eV) and the presence of satellite peaks at about 5 eV higher than the binding energy of the parent signal. This observation is consistent with that of Korányi et al. [38]. For the fresh catalysts (Fig. 5(a) and (b)), bands at 852.7–853.4 eV and at 129.3–130.1 eV are observed, which can be assigned to the $Ni^{\delta+}$ and $P^{\delta-}$ species, respectively. The $Ni^{\delta+}$ binding energies are slightly higher than reported values for Ni metal (852.5–852.9 eV) and lower than those reported for Ni in NiO (853.5–854.1 eV), indicating that the Ni in Ni_2P and $Ni_{12}P_5$ bears a partial positive charge [6]. The $P^{\delta-}$ binding energies are below the value reported for elemental phosphorus (130.2 eV), consistent with the transfer of electron density from Ni to P in unsupported and silica-supported Ni_2P or $Ni_{12}P_5$ so that the phosphorus bears a partial negative charge [6]. The bands at 856.1–857.2 eV and at 134.0–134.5 eV are assigned to the Ni^{2+} and P^{5+} (phosphate) species, respectively. The P^{5+} binding energy is in good agreement with a value reported for P (134.3 eV) in $Ni_3(PO_4)_2$ [40], while the Ni^{2+} binding energies are similar to the binding energy of those reported for Ni (855.6–856.6 eV) in $Ni(OH)_2$ [41]. The Ni^{2+} and P^{5+} species correspond to the possible interaction of Ni^{2+} ions with phosphate ions (PO_4^{3-}), as a consequence of superficial passivation [35]. Moreover, a broad shake-up peak at approximately 5.0 eV higher than that of the Ni^{2+} species can be observed [31]. These satellite peaks are due to divalent species [42,43], although, in the literature, they have also been assigned to trivalent and oxysulfided nickel species [19,44]. Other broad peaks, centered at higher binding energy, are assigned to the Ni 2p signal from oxidized Ni [45]. The spent catalysts, obtained after 12 h HDS reaction, were also studied by XPS and the results are shown in Fig. 5(c) and (d). In contrast with the corresponding fresh catalyst, the $Ni^{\delta+}$ binding energy of the spent catalyst shifts to a slightly higher value, while the $P^{\delta-}$ shifts to a slightly lower value. This shift of binding energy implies that the structure of the surface of catalysts has changed during the HDS reaction. This surface modification of Ni_2P during the HDS reaction has been regarded as a consequence of the presence of a superficial phosphosulfide, with a stoichiometry represented by $Ni_xP_yS_z$ [10,46,47]. The S 2p signal analysis for spent catalysts reflects that all the catalysts possess two sulfur 2p bands located at 161.4–161.9 eV and 168.0–178.5 eV, which are due to sulfide and sulfate species respectively [48]. X. Duan and Cecilia et al. [19,49] have also observed two sulfur bands on a H_2S-passivated Ni_2P/MCM-41 catalyst which was active and stable in DBT HDS reaction. These authors have assigned the band over 168.0 eV as consequence of the oxidation of sulfur species retained on the Ni_2P/MCM-41 catalyst surface. Therefore it is reasonable to expect the partial oxidation of the sulfur species is responsible for the band at 161.4–161.9 eV in Fig. 5(e).

XPS analyses were also used to calculate the surface atomic ratios (Table 2). The theoretical P/Ni ratios of the Ni-P(0.5)/MCM, Ni-P(2)/MCM, Ni-P(6)/MCM, and Ni-P(10)/MCM fresh catalysts would be 0.4–0.6, assuming that excess phosphorous would be washed by the ethanol and carbon tetrachloride. However, the P/Ni ratios are much higher than the theoretical value, the high P/Ni ratios found for the catalysts confirms that on the surface there is an enrichment of phosphorous, although it is essentially present as PO_4^{3-} forming a passivation layer in the surface of Ni_2P and $Ni_{12}P_5$ particles. The bulk crystal structure of Ni_2P belongs to space group $P\bar{6}2m$ with $a = b = 0.5859$ nm and $c = 0.3382$ nm [50] Along the (0 0 0 1) direction, the bulk structure consists of two different alternating stoichiometric planes, namely Ni_3P and Ni_3P_2. The density functional theory (DFT) studies showed that the Ni_3P_2 terminated surface is more stable than the Ni_3P terminated surface [8,51], where as STM and PEEM studies showed that a substantial amount of the Ni_2P surface is terminated with the Ni_3P structure [8,52–54]. Hernandez et al. [55] found that the fundamental surface structure of Ni_2P (0 0 0 1) surface is composed of approximately 80% of Ni_3P_P (Ni_3P_2 covered with P at the Ni three-fold hollow sites) and 20% of bare Ni_3P_2, and the surface was terminated with P atoms. Hence, it is reasonable to speculate that the phenomenon rich in phosphorous on surface is the inner characteristic of Ni_2P. Moreover, the XRD also shows that the pure Ni_2P phase cannot be obtained for sample with the initial P/Ni molar ratio of 0.5. The spent catalysts show a decrease in the P/Ni molar ratios, particularly the Ni-P(0.5)/MCM catalyst, which suffers an important loss in phosphorous. The P/Ni molar ratios of the spent catalysts (shown in Table 2) indicate that although some phosphorous have lost during HDS reaction, the catalysts surface is still enriched in phosphorous. The Ni 2p spectra of all the catalysts clearly show the $Ni^{\delta+}/\sum Ni$ is lower than 0.4, which indicates a much higher proportion of superficial nickel atoms is at oxidation state. The Ni-P(2)/MCM catalysts show lower Ni/Si atomic ratio than that of Ni-P(2)/MCM-T catalyst, indicating the catalysts prepared by the solution-phase synthesis have good dispersion of nickel on support or more Si atoms exposed at the surface of the solution-phase synthesized catalysts due to the lower P coverage compared with the catalysts obtained by TPR.

It should be noted that sulfur was detected in the spent catalysts, which may be due to formation of a superficial phosphosulfide ($Ni_xP_yS_z$) on the catalysts. Oyama et al. [7] identified a surface phosphosulfide phase by XRD and EXAFS on top of a Ni_2P core, they suggested that this may be an active phase of the Ni_2P/SiO_2 catalysts, and the maximum sulfur level was reckoned to be 5 mol% of the phosphorus content. Using the DFT calculations, Nelson et al.

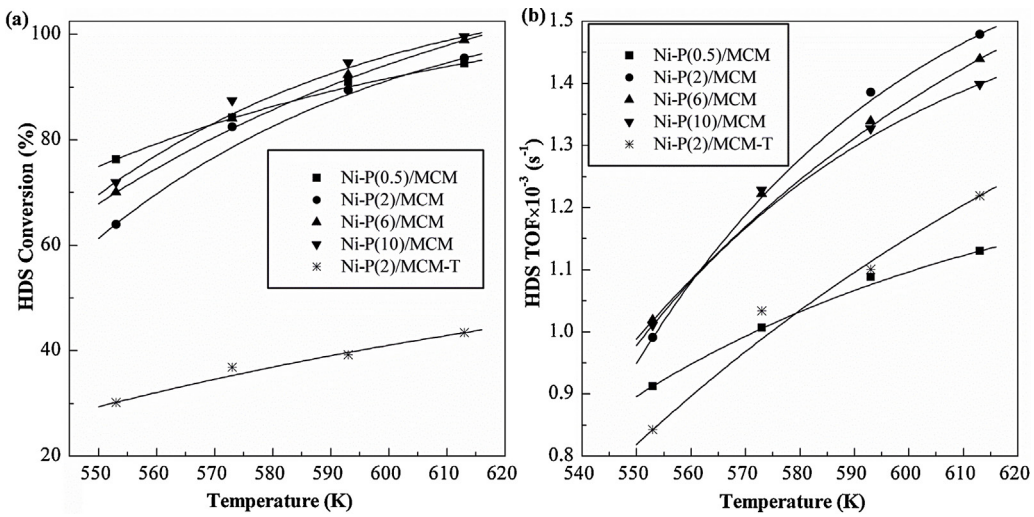

Fig. 6. HDS conversion and TOF for DBT HDS at different reaction temperature over Ni-P(X)/MCM and Ni-P(2)/MCM-T catalysts (3.0 MPa, WHSV = 4 h^{-1}, H_2/oil = 500 (v/v)).

[47] studied the replacement of up to 50% of surface phosphorus of the bulk Ni_2P by sulfur and suggested that surface Ni_3PS is the actual active phase of Ni_2P for the hydrotreatment reactions. Korányi et al. [38] found a superficial phosphosulfide with a composition $Ni_{2.4}P_{1.0}S_{0.24}$ for the catalyst pretreated by H_2S. In this paper, we found the composition of the surface active-phases of spent Ni-P(2)/MCM, Ni-P(6)/MCM and Ni-P(10)/MCM were $NiP_{2.2}S_{1.97}$, $NiP_{2.2}S_{1.84}$ and $NiP_{2.3}S_{1.96}$, respectively. Considering that our catalysts were pretreated with H_2 rather than by H_2S, we can conclude that the high sulfur content in the superficial phosphosulfide phase may be due to adsorbed sulfur species.

3.2. HDS activity

Fig. 6(a) shows the variations of DBT conversion with temperature during DBT HDS catalyzed by Ni-P(X)/MCM and Ni-P(2)/MCM-T catalysts. The DBT HDS conversion of Ni-P(2)/MCM-T is about 30% at 553 K, and this increases with increasing reaction temperature. At 613 K, the DBT conversion reached 43%. Clearly, the DBT conversion using Ni-P(X)/MCM catalysts is dramatically higher than with Ni-P(2)/MCM-T. The Ni-P(X)/MCM catalysts also show that the activity increases with increasing reaction temperature; the Ni-P(6)/MCM and Ni-P(10)/MCM catalysts produce conversion close to 100% at 613 K. It is noteworthy that the Ni-P(0.5)/MCM catalyst, containing mainly the $Ni_{12}P_5$ phase, also shows a higher HDS activity than Ni-P(2)/MCM-T, although it has been reported that the HDS activity of $Ni_{12}P_5$ catalysts was lower than that of Ni_2P catalysts under the same conditions [55]. The high HDS activity observed in the Ni-P(X)/MCM catalysts may be due to the high dispersion of the active phase and low coverage of phosphorus on the surface of these catalysts. The CO uptake shows that the Ni-P(X)/MCM catalysts can adsorb much more CO than Ni-P(2)/MCM-T, indicating that Ni-P(X)/MCM can offer more exposed metal sites for HDS reaction. The adsorption states of DBT on the catalysts are supposed to be of two kinds: one is end-on through the adsorption of sulfur atoms, the other is flat, involving the π-electrons of DBT molecules [56]. The end-on adsorption orientation yields the DDS pathway, while the flat orientation leads to the formation of HYD pathway products. DFT calculations indicated that the sulfur atoms in DBT are positively charged and represent the main nucleophilic attack center [57]. Hence, a greater number of metal sites benefits the DBT HDS reaction. The Ni-P(X)/MCM catalysts show a very constant degree of HDS conversion over the range 513–613 K. The weak effect of the phosphorus content on the conversion of these catalysts indicates that the reaction occurs principally on metal centers and the effect of ensemble size on reactivity is modest. Hence, the reaction is structurally insensitive. A similar observation was reported by Oyama et al. [31], in which the authors studied the effect of the P/Ni molar ratio on the HDS and hydrodenitrogenation (HDN), and found a strong dependence for the HDN of quinoline but only a very weak dependence for the HDS of DBT.

The DBT conversion and CO uptake of spent catalysts have been used to calculate the HDS TOF for the catalysts. The value of HDS TOF for each catalyst increased with temperature (Fig. 6(b)), suggesting that the DBT HDS over Ni_2P and $Ni_{12}P_5$ catalysts is a thermodynamically favorable reaction. Of all catalysts, the Ni-P(2)/MCM, Ni-P(6)/MCM and Ni-P(10)/MCM display nearly the same TOF, the value of which is higher than that of Ni-P(2)/MCM-T. However, a low TOF was observed for the Ni-P(0.5)/MCM catalyst. This indicates that the metal sites are not directly involved in the HDS reaction, since the Ni-P(0.5)/MCM catalyst shows the highest CO uptake value of the catalysts, which means that it has the largest numbers of metal sites. Indeed, it is accepted that metal sites simply provide the initial active sites, and the real active phase is a nickel phosphosulfide produced from the HDS reaction [5,7,31].

With regard to the selectivity of the different reaction products, seven products are detected (as shown in Scheme 1), but the biphenyl (BP) and cyclohexylbenzene (CHB) are in the majority. The transformation of DBT occurs through two parallel pathways: (1) direct desulfurization (DDS), which yields BP and then BP hydrogenation yields CHB, and (2) desulfurization after hydrogenation (HYD), which yields tetrahydrodibenzothiophene (TH-DBT) and then CHB. Because the transformation of BP to CHB is negligible in the presence of DBT, BP selectivity is used as a measure of DDS pathway, and CHB represents the HYD pathway. Fig. 7 illustrates the variations of BP and CHB yields with reaction temperature over Ni-P(X)/MCM and Ni-P(2)/MCM-T catalysts. For all the samples, the yield of BP is much higher than that of CHB, indicating that DBT mainly removed by the DDS pathway over the catalysts, which can be attributed to the DBT HDS reaction is structure insensitive [31]. It has been reported a lower hydrogenation activity of phosphides, with regards to sulfides, indicating a more effective use of hydrogen in the HDS reaction [5]. A study using the Ni-Mo-P/SiO_2 catalyst underlined the importance of nickel sites in Ni_2P in the catalytic activity, concluding that HDS reaction mainly occurred on Ni sites, this being one of the properties that makes phosphide catalysts different from either sulfide, carbide or nitride catalysts

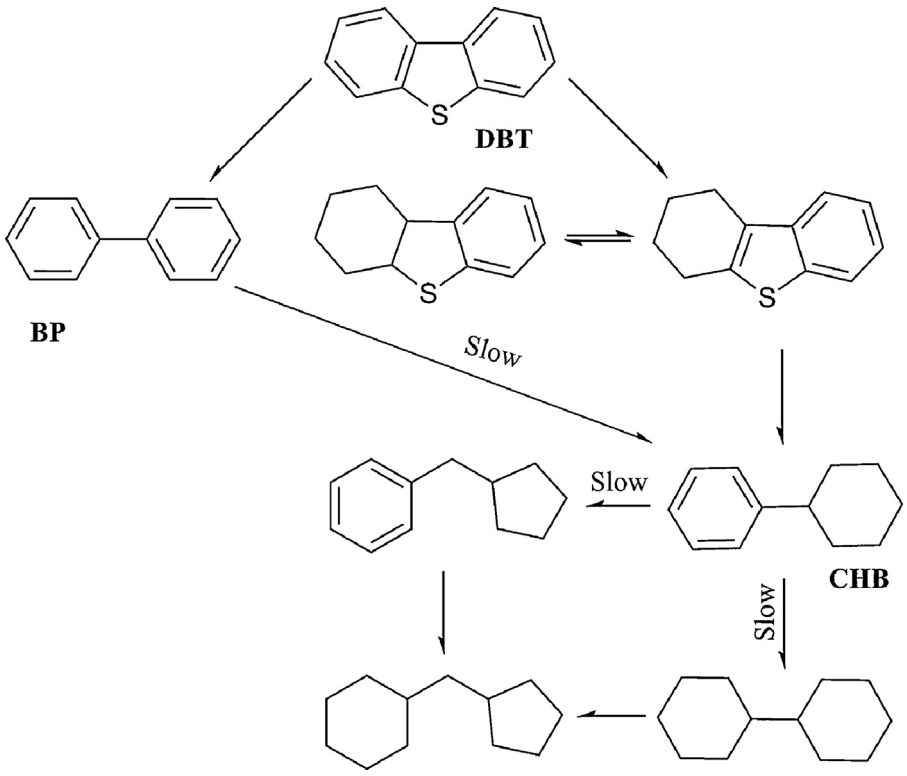

Scheme 1. The HDS reaction network of DBT over Ni_2P catalyst.

[10]. The selectivity to CHB of Ni-P(X)/MCM is higher compared with that of Ni-P(2)/MCM-T catalysts, which may be attributed to the smaller active crystal particles formed in Ni-P(X)/MCM catalysts and produce more Ni(2) sites so as to provide higher HYD selectivity. As reported by the literature [58], there are two types of sites in Ni_2P, Ni(1) sites with tetrahedral coordination and Ni(2) sites with square pyramidal coordination, both Ni(1) and Ni(2) sites are present on large crystallites but that the Ni(2) sites are more numerous on the more highly dispersed samples. The lower coordination Ni(1) sites are responsible for desulfurization by the DDS pathway by taking on a sulfur atom while the Ni(2) sites are the high-activity sites that carry out HDS by the hydrogenation (HYD) route. Hence, we conclude that the acceleration of the HYD pathway over the Ni-P(X)/MCM catalysts must be associated with the dispersion of active crystal particles. It should be noted that the role of the Ni(1) and Ni(2) sites are to provide just the initial state for the HDS active sites, because the surface of catalyst should be sulfided and some P atoms are replaced by S atoms during reaction [58]. On the other hand, the selectivity of BP increases with increasing reaction temperature during DBT HDS over all the catalysts, suggesting that the distribution of HDS products over the Ni-P(2)/MCM-T and Ni-P(X)/MCM catalysts is sensitive to temperature and the DDS activity can be enhanced by increasing reaction temperature. The Ni-P(0.5)/MCM catalyst shows the highest CHB selectivity among the Ni-P(X)/MCM catalysts, indicating the $Ni_{12}P_5$ phase has higher HYD activity than Ni_2P phase.

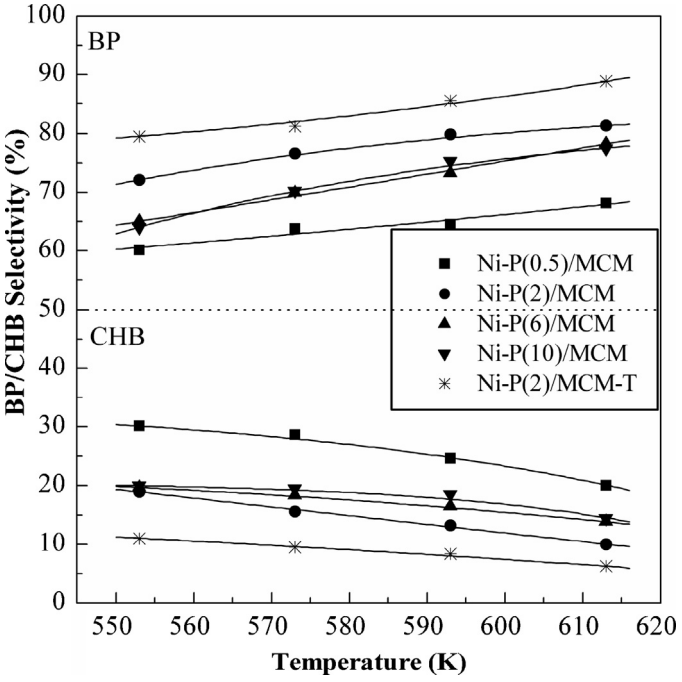

Fig. 7. BP and CHB selectivities at different reaction temperature over Ni-P(X)/MCM and Ni-P(2)/MCM-T catalysts (3.0 MPa, WHSV = 4 h^{-1}, H_2/oil = 500 (v/v)).

Fig. 8 shows the DBT conversion and yield values versus reaction time for Ni-P(6)/MCM catalyst. The reaction temperature chosen was 613 K. It can be seen from Fig. 8 that the activity of catalyst increases gradually in the initial 10 h, and the conversion of DBT is close to 99% after 12 h and stays constant for 120 h without activity loss under the given reaction conditions. The catalyst improves its catalytic capacity during the initial time on stream, which suggests that there is a formation of an intermediate phase which is more active than Ni_2P. The surface modification of Ni_2P phase during the HDS reaction and the explanation of its excellent behavior with initial time on stream have been considered in the literature as consequence of the presence of a superficial phosphosulfide as active phase with a stoichiometry represented by NiP_xS_y [10,46,47]. Our XPS of the spent Ni-P(6)/MCM sample shows a superficial phosphosulfide with a composition of $NiP_{2.2}S_{1.84}$. Further, Ni_2P has better sulfur resistance than metal carbides and nitrides which transform

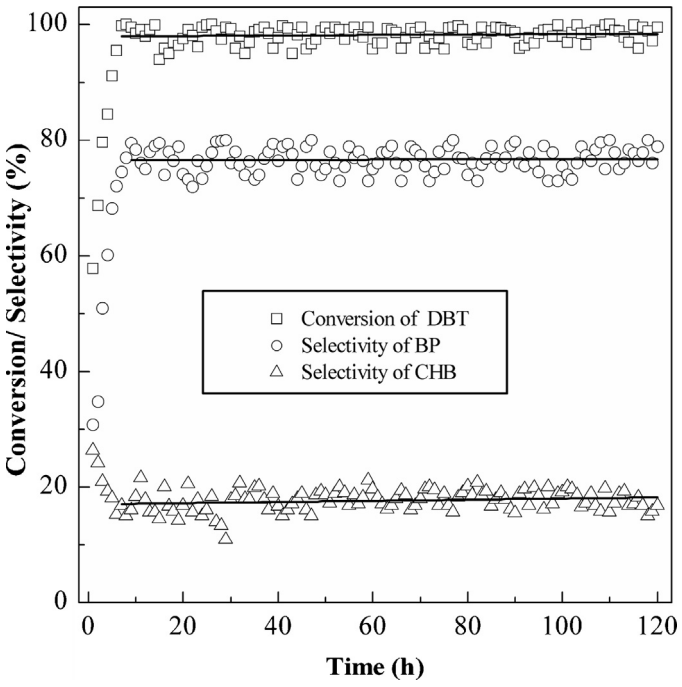

Fig. 8. DBT conversion and selectivity of BP and CHB as a function of time on stream for Ni-P(6)/MCM catalyst at 613 K (613 K, 3.0 MPa, WHSV = 4 h^{-1}, H_2/oil = 500 (v/v)).

into metal sulfides with high activity under HDS conditions [15]. Fig. 8 shows the conversion of DBT is still more than 99% in the case of DBT content in feed is as high as 1 wt.%. Although the surface of Ni_2P takes up sulfur atoms under HDS conditions, the kernel of the Ni_2P particles remains intactness [37,59]. The XRD shows there is no sulfide phase (no distinct peak corresponding to the sulfide phase is seen in Fig. 2 of the spent catalyst) in the spent catalyst, which also indicates the kernel of the Ni_2P particles is stable. Again, the selectivity of BP is always higher than CHB during the 120 h, indicating the DBT HDS over Ni_2P catalyst tends toward DDS way.

4. Conclusions

A novel low-price solution-phase method for preparing a supported Ni_2P catalyst using mild conditions is reported. This uses nickel acetylacetonate ($Ni(acac)_2$) as a nickel precursor and low price triphenylphosphine (TPP) as a phosphorus precursor to prepare the Ni_2P supported on mesoporous MCM-41 catalysts at 603 K in a N_2 atmosphere. The experimental results definitely indicate that the proposed solution-phase approach is feasible. The approach does not require such a high reduction temperature as the TPR method, so providing an alternative way to synthesize Ni_2P catalysts with high HDS activity. XRD shows that as the synthesis temperature is increased, the formation of the crystalline phase follows the order Ni, $Ni_{12}P_5$, and Ni_2P. The phosphorus content has a profound effect on the formation of crystalline phases The precursor with initial P/Ni molar ratio of 0.5 yielded a catalyst containing predominantly $Ni_{12}P_5$ phase with a little Ni_2P, and a high initial P/Ni molar ratio favors the formation of the Ni_2P phase and its dispersion. The XPS indicates that there is an enrichment of phosphorus on the surface of the catalysts. During the HDS reaction, a superficial phosphosulfide phase is formed on the surface of the catalyst, which leads to higher activity than Ni_2P. The catalyst prepared by the proposed solution-phase approach showed higher activity than the catalyst prepared by a conventional TPR method. This can be attributed to the better dispersion and lower coverage of phosphorus over the surface of the catalysts. The DBT HDS tests showed that the DBT conversion increased with reaction temperature, and DBT mainly desulfurizes by the DDS pathway over the catalysts. A catalyst stability test for Ni-P(6)/MCM over 120 h indicated that the Ni_2P catalyst is highly sulfur resistant. The conversion of DBT was maintained at 99% throughout the test time with model fuel which contents DBT as high as 1 wt.% at 613 K, 3.0 MPa, WHSV = 4 h^{-1} and H_2/oil = 500 (v/v)).

Acknowledgments

The authors acknowledge the financial supports from the National Natural Science Foundation of China (21276048) and the Natural Science Foundation of Heilongjiang Province (ZD201201).

References

[1] R. Prins, Adv. Catal. 46 (2001) 399.
[2] M. Sun, D. Nicosia, R. Prins, Catal. Today 86 (2003) 173.
[3] S.K. Bej, S.K. Maity, U.T. Turaga, Energy Fuels 18 (2004) 1227.
[4] X. Wang, P. Clark, S.T. Oyama, J. Catal. 208 (2002) 321.
[5] S.T. Oyama, J. Catal. 216 (2003) 343.
[6] S.J. Sawhill, D.C. Phillips, M.E. Bussell, J. Catal. 215 (2003) 208.
[7] S.T. Oyama, X. Wang, Y.K. Lee, W.J. Chun, J. Catal. 221 (2004) 263.
[8] P. Liu, J.A. Rodriguez, T. Asakura, J. Gomes, K. Nakamura, J. Phys. Chem. B 109 (2005) 4575.
[9] D. Kanama, S.T. Oyama, S. Otani, D.F. Cox, Surf. Sci. 552 (2004) 8.
[10] F. Sun, W. Wu, Z. Wu, J. Guo, Z. Wei, Y. Yang, Z. Jiang, F. Tian, C. Li, J. Catal. 228 (2004) 298.
[11] Y. Shu, Y.K. Lee, S.T. Oyama, J. Catal. 236 (2005) 112.
[12] J. Guan, Y. Wang, M. Qin, Y. Yang, X. Li, A. Wang, J. Solid State Chem. 182 (2009) 1550.
[13] Y. Shu, S. Ted Oyama, Carbon 43 (2005) 1517.
[14] G. Berhault, P. Afanasiev, H. Loboue, C. Geantet, T. Cseri, C. Pichon, C. Guillot Deudon, A. Lafond, Inorg. Chem. 48 (2009) 2985.
[15] S.F. Yang, C.H. Liang, R. Prins, J. Catal. 237 (2006) 118.
[16] X. Wang, F. Wan, Y. Gao, J. Liu, K. Jiang, J. Cryst. Growth 310 (2008) 2569.
[17] K. Mi, Y. Ni, J. Hong, J. Phys. Chem. Solids 72 (2011) 1452.
[18] H. Loboué, C. Guillot-Deudon, A.F. Popa, A. Lafond, B. Rebours, C. Pichon, T. Cseri, G. Berhault, C. Geantet, Catal. Today 130 (2008) 63.
[19] J.A. Cecilia, A. Infantes-Molina, E. Rodríguez-Castellón, A. Jiménez-López, J. Catal. 263 (2009) 4.
[20] A. Wang, M. Qin, J. Guan, L. Wang, H. Guo, X. Li, Y. Wang, R. Prins, Y. Hu, Angew. Chem. Int. Ed. 47 (2008) 6052.
[21] Y. Zhao, M. Xue, M. Cao, J. Shen, Appl. Catal. B-Environ. 104 (2011) 229.
[22] G.J. Shi, J.Y. Shen, J. Mater. Chem. 19 (2009) 2295.
[23] J. Wang, A.C. Johnston-Peck, J.B. Tracy, Chem. Mater. 21 (2009) 4462.
[24] R.K. Chiang, R.T. Chiang, Inorg. Chem. 46 (2007) 369.
[25] K. Senevirathne, A.W. Burns, M.E. Bussell, S.L. Brock, Adv. Funct. Mater. 17 (2007) 3933.
[26] K.A. Gregg, S.C. Perera, G. Lawes, S. Shinozaki, S.L. Brock, Chem. Mater. 18 (2006) 879.
[27] C. Qian, F. Kim, L. Ma, F. Tsui, P. Yang, J. Liu, J. Am. Chem. Soc. 126 (2004) 119.
[28] J. Park, B. Koo, K.Y. Yoon, Y. Hwang, M. Kang, J.G. Park, T. Hyeon, J. Am. Chem. Soc. 127 (2005) 8433.
[29] S.C. Perera, G. Tsoi, L.E. Wenger, S.L. Brock, J. Am. Chem. Soc. 125 (2003) 13960.
[30] H.I. Meléndez-Ortiz, L.A. García-Cerda, Y. Olivares-Maldonado, G. Castruita, J.A. Mercado-Silva, Y.A. Perera-Mercado, Ceram. Int. 38 (2012) 6353.
[31] S.T. Oyama, X. Wang, Y.-K. Lee, K. Bando, F.G. Requejo, J. Catal. 210 (2002) 207.
[32] V. Teixeira da Silva, L.A. Sousa, R.M. Amorimb, L. Andrini, S.J.A. Figueroa, F.G. Requejo, F.C. Vicentini, J. Catal. 279 (2011) 88.
[33] H.R. Seo, K.S. Cho, Y.K. Lee, Mater. Sci. Eng. B 176 (2011) 132.
[34] S. Carenco, Ć. Boissière, L. Nicole, C. Sanchez, P.L. Floch, N. Mézailles, Chem. Mater. 22 (2010) 1340.
[35] H. Song, M. Dai, Y.T. Guo, Y.J. Zhang, Fuel Process. Technol. 96 (2012) 228.
[36] I.I. Abu, K.J. Smith, Appl. Catal. A 328 (2007) 58.
[37] K.A. Layman, M.E. Bussell, J. Phys. Chem. B 108 (2004) 10930.
[38] T.I. Korányi, Z. Vít, D.G. Poduval, R. Ryoo, H.S. Kim, E.J.M. Hensen, J. Catal. 253 (2008) 119.
[39] Y.K. Lee, Y. Shu, S.T. Oyama, Appl. Catal. A 322 (2007) 191.
[40] R. Franke, T. Chasse, P. Streubel, A. Meisel, J. Electron. Spectrosc. 56 (1991) 381.
[41] P. Dufresne, E. Payen, J. Grimblot, J.P. Bonnelle, J. Phys. Chem. 85 (1981) 2344.
[42] D. Eliche-Quesada, J. Merida-Robles, P. Maireles-Torres, E. Rodriguez-Castellon, A. Jimenez-Lopez, Langmuir 19 (2003) 4985.
[43] J.N. Kuhn, N. Lakshminarayanan, U.S. Ozkan, J. Mol. Catal. A-Chem. 282 (2008) 9.
[44] L. Song, S. Zhang, Q. Wei, Catal. Commun. 12 (2011) 1157.
[45] N. Escalona, J. Ojeda, P. Baeza, R. Garcia, J.M. Palacios, J.L.G. Fierro, A.L. Agudo, F.J. Gil-Llambias, Appl. Catal. A 287 (2005) 47.
[46] T. Kawai, K.K. Bando, Y.K. Lee, S.T. Oyama, W.J. Chun, K. Asakura, J. Catal. 241 (2006) 20.
[47] A.E. Nelson, M. Sun, A.S.M. Junaid, J. Catal. 241 (2006) 180.
[48] L. Qiu, K. Zou, G. Xu, Appl. Surf. Sci. 266 (2013) 230.

[49] X. Duan, Y. Teng, A. Wang, V.M. Kogan, X. Li, Y. Wang, J. Catal. 261 (2009) 232.
[50] S. Rundqvist, Acta Chem. Scand. 16 (1962) 992.
[51] Q. Li, X. Hu, Phys. Rev. B 74 (2006) 035414.
[52] M.G. Moula, S. Suzuki, W.J. Chun, S. Otani, S.T. Oyama, Q. Li, K. Asakura, Chem. Lett. 35 (2006) 90.
[53] S. Suzuki, G.M. Moula, T. Miyamoto, Y. Nakagawa, K. Kinosthita, K. Asakura, S.T. Oyama, S. Otani, J. Nanosci. Nanotechnol. 9 (2008) 195.
[54] Q. Guan, X. Cheng, R. Li, W. Li, J. Catal. 299 (2013) 1.
[55] A.B. Hernandez, H. Ariga, S. Takakusagi, K. Kinoshita, S. Suzuki, S. Otani, S.T. Oyama, K. Asakura, Chem. Phys. Lett. 513 (2011) 48.
[56] M.J. Girgis, B.C. Gates, Ind. Eng. Chem. Res. 30 (1991) 2021.
[57] C.I. Sainz-Díaz, M. Francisco-Márquez, A. Vivier-Bunge, Theor. Chem. Acc. 125 (2010) 83.
[58] S.T. Oyama, Y.K. Lee, J. Catal. 258 (2008) 393.
[59] Z. Wu, F. Sun, W. Wu, Z. Feng, C. Liang, Z. Wei, C. Li, J. Catal. 222 (2004) 41.